Modeling Uranium Uptake in Fossilized Teeth and Bones: Insight into Potential for Long-Term Uranium Waste Storage in Phosphates

Ethan Sontarp

Abstract

Oxidized uranium (U) is soluble in groundwater and can be incorporated in or adsorbed to porous materials it encounters in the environment. In the early stages of fossilization, mammal teeth and bones provide this environment through bacterial decay and mineralization of the previously living tissue. The purpose of this study is to quantitatively model the uptake of uranium in porous biomaterials to 1) predict age of fossilization for samples whose origin is unknown, and 2) to understand the systematics of an exponential falloff uranium uptake in phosphates in order to improve the function of nuclear waste remediation tactics. Laser Ablation Inductively Coupled Plasma Mass Spectrometry (LA-ICP-MS) was utilized to determine isotopic ratios and ultimately calculate the isotopic age for a small elemental map spanning several of the hydroxyapatite-bearing biomaterials. Uranium concentrations were in the thousands of ppm for sections of dentine and under 100 ppm for sections of enamel. A model was devised based off the isotopic age equation to describe the uptake history of uranium in several fossilized biomaterials. Parameters for the model were described by an exponential fall off of uranium (U) uptake, with the initial U being zero and lead (Pb) only being produced as a product of decay. Simulated and measured data assured a good fit for the model's predictive property. Conjugate gradient technique was utilized to solve for local values of initial uptake, e-folding time, and predicted age, with the e-folding time for the bone sample being 1.3 Ma, and the tooth 0.9 Ma, respectively. These provide insight into the process of uranium uptake in porous biomaterials to further the knowledge of nuclear waste sequestration, as both porous materials had a rapid uptake history. Porous phosphates are worthy materials for the remediation of high concentrations of uranium waste and are able to hold uranium for millions of years of time, even under destructive geological conditions.

1. Introduction:

1.1. Uranium Sequestration

Nuclear meltdowns and waste mishandling have left some of the groundwater supply contaminated with radioactive uranium, and efforts to combat this have resulted in studies about nuclear waste remediation which are relatively short in terms of the geologic time scale (Crowley, 1997). The process by which uranium is taken up and stored in a porous material is integral to the study of nuclear waste remediation. Uranium itself is soluble in the oxidized state and very easily percolates into the water supply from the solid state, as seen in Equation 1 with the dissociation of the mineral coffinite in water (Sanding et al, 1992).

$$USiO_{4\,(s)} + H_2O_{(l)} \rightarrow (UO_2)^{2+}{}_{(s)} + SiO_{2(s)} + H_2O_{(l)} \quad \textbf{(1)}$$

Under certain reducing conditions, uranium, in the form of the polyatomic ion uranyl, UO_2^{2+} can replace calcium ions and become immobilized inside a porous biogenic material (Sharp et al, 2011). In addition, uranium can precipitate inside of these materials if open pore space is available. Uranium itself naturally occurs in minute levels due to the presence of decayed vegetation, which fosters an oxidizing environment key to its mobilization (Banning et al, 2013). Therefore, uranium can become incorporated easily into aquifers via groundwater flow. Furthermore, the element can be present in the environment as a harmful byproduct of nuclear energy production. In high concentrations, uranium poses a threat to the freshwater ecosystem, exposing the flora and fauna to high dosages of damaging radioactive decay (Matthews et al, 2009).

To prevent the introduction of chemically unbound uranium to an ecosystem, phosphate materials are often used to sequester the radioactive element (Martinez et al, 2014). The hexavalent uranyl ion, $(UO_2)^{2+}$, can be effectively immobilized by reacting with the calcium phosphate mineral, hydroxyapatite, present in mammal teeth and bones, as seen in Equation 2 (Wellman et al, 2008).

$$2(UO_2)^{2+}{}_{(aq)} + Ca_5(PO_4)_3(OH)_{(s)} + nH_2O_{(l)} \rightarrow Ca[UO_2PO_4]_2 \cdot nH_2O_{(s)} + PO_4^{3-}{}_{(aq)} \quad \textbf{(2)}$$

Uptake laws are used to model the chemical addition of uranium into a remediation system and provide insight into the immobilization of the element over time. Previous uptake laws have described the uptake of uranium in the porous dentine and rigid enamel of mammalian teeth yet have not assessed the uptake rate with regard to a system's isotopic signature (Pike and Hedges, 2001).

The potential for hydroxyapatite to be utilized as an effective Permeable Reactive Barrier (PRB) remains a promising and cost-effective alternative to the nuclear waste containers being evaluated by the

Yucca Mountain Site Characterization Project (Gdowski, 1997). These containers employ a high quantity of corrosion-resistant titanium alloy and reactive borosilicate glass to enclose radioactive uranium waste at the designated Yucca Mountain site, which serves as an archetype for nuclear waste remediation (Gin et al, 2013). A limitation to the Yucca Mountain project, however, is that it lacks the predictive factor of a site which has immobilized uranium waste for an extended period. The purpose of this study is to simulate uranium uptake and immobilization in hydroxyapatite fossils as a predictive model for the behavior of the radioactive waste over a timescale of fourteen million years. This will provide insight into the extent and duration of uranium waste remediation strategies.

1.2. Geologic Setting

The Barstow Formation, located in the central Mojave Desert of Southern California, contains an abundance of well-preserved fossils. It was created during the Miocene Epoch (23.0-5.3 Ma) and contains several layers of volcanic ash tuff interlaced with lacustrine sedimentary rock (Woodburne et al, 1990). The distinct layers of tuff are precisely dated and therefore serve as calibration points for the discovered fossils.

The Barstovian North American Land Mammal Age (16.3-13.6 Ma) is defined by mammalian fossils located in its various layers and provides a reference for all study of mammal evolution in North America. Most rodent and camel fossils are found in the upper middle section of the formation, along with the horse genus *Scaphohippus*. Horse teeth differ from human teeth in that they are hypsodonts, or high crowning, and contain alternating layers of enamel and dentine. These hypsodonts developed shortly before the genus *Scaphohippus* evolved, due to the transition of North America from a forested to grassland environment around 15 Ma. This can be evidenced by the transition of grasses from a simpler C3 photosynthetic system to C4 photosynthesis (Wang et al, 1994).

1.3. Case Study Sample Set

The samples of a horse tooth and bone used in this experiment were found in the Barstow Formation's Hell Gate Basin. This basin is situated below Robbins Quarry, which is radiometrically dated at 13.86 ± 0.65 Ma (Woodburne et al, 1990). Each of the samples were assumed to have undergone diagenesis shortly after their burial and have taken up radiometric uranium (Kohn, 1999). Oftentimes, rare-earth elements will replace calcium in calcium phosphate, which composes most of the enamel and dentine in a tooth. Enamel is about 96% calcium phosphate ($Ca_3(PO_4)_2$) and dentine is about 70%. Through uptake and leaching processes, uranium most likely entered the dentine through the decaying pulp. For this reason, dentine may be more useful in the process of isotope dating than enamel. Bones are also made up of calcium phosphate, along with collagen, making them comparable to teeth. The unstable

U-238 and U-235 isotopes have since decayed over millions of years into Pb-206 and Pb-207 isotopes along two decay chains, allowing the ratios to be compared following the isotopic age equation (Hirata and Nesbitt, 1995).

For this case study, two samples of hydroxyapatite-bearing biomaterials, one bone and one tooth, respectively, were subjected to experimental processes. Sample 1A is an intact *Scaphohippus intermontanus* tooth uncovered 13 meters below Robbins Quarry and Sample 1C is an intact calcaneus bone of the same species uncovered 7 meters under Robbins Quarry. Both of these samples contain distinct layering of inorganic material and mineralization in the spaces where there was formerly organic material. In the tooth, the dentine regions behave most like a synthetic compound used to sequester nuclear waste, as it is far more porous. Similarly, the spongy bone portion of the bone behaves as an ideal material for the containment of nuclear waste.

Figures 1a & 1b. Sample 1A is a tooth and sample 1C is a bone which originate from *Scaphohippus intermontanus*. Both were discovered in the Barstow Formation of Southern California. For sample 1A, the darker sections contain enamel and the lighter sections contain dentine. Inner dentine refers to the section of lighter material in the center of the tooth, and outer dentine refers to the same material surrounding the inner section of enamel. For sample 1C, the darker sections contain cortical bone and the lighter sections are pores of former organic material interlaced with spongy bone.

2. **Methods:**

2.1. Experimental Methods

Tooth samples were first placed in Beuhler Epoxicure epoxy, utilizing a 4:1 ratio of resin to hardener. The epoxy was used to provide structure for the teeth and to prevent fracturing when cut. The bone samples were determined to be sturdy enough to cut without epoxy. All samples were then sliced into thick sections of about 5 mm using a Beuhler IsoMet slow saw. One side of each of the thick sections was polished on a glass plate using a sequence of 120, 320, 400, and 600 grits. The samples were moved in figure-8's for 5 minutes with each grit size and rinsed between every polishing. Afterwards, they were washed and dried thoroughly to reveal a smooth surface. Each of the thick sections were then scanned and

imaged. These images were used to determine the structure of the layers in the teeth and bones. Referencing a synchrotron image of the elemental composition of the tooth, which was obtained from sample 1A, the areas of interest were determined for analysis. The image highlighted the differences in elemental compositions between sections of the tooth. The dentine, specifically the inner portions, has the highest uranium concentration, whereas the enamel contains relatively little uranium in comparison. Due to the high concentrations of uranium present in the sample, U/Pb isotopic dating was implemented to obtain information about the uranium containment properties of the biomaterials.

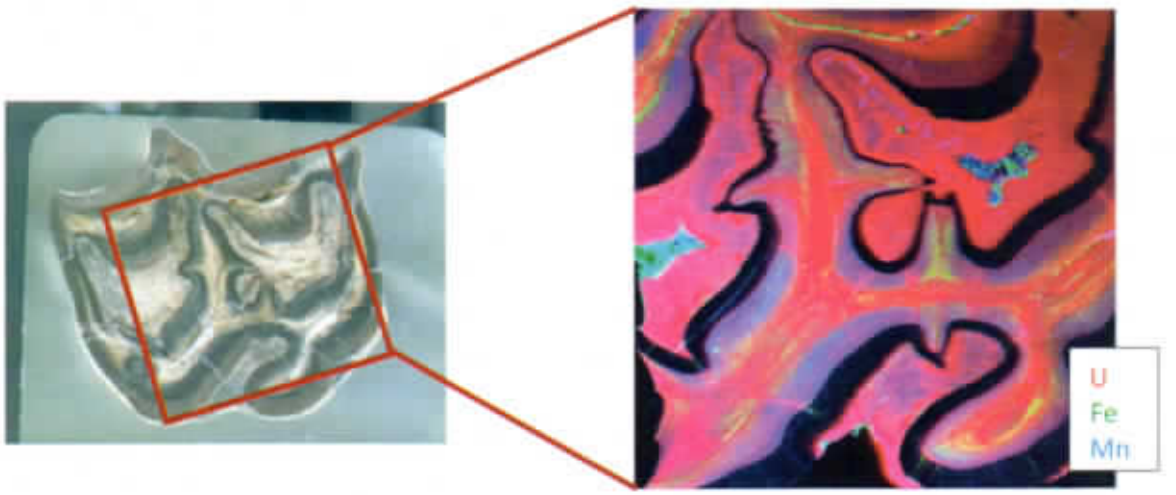

Figure 2. Map image of the primary sample using X-Ray Diffraction at the National Synchrotron Light Source II (NSLS II). Image obtained by Alvin Acerbo, 2018. Elements in high concentration were mapped to reveal the structure and localities inside the tooth. Uranium is represented in red, iron in green, and manganese in blue.

2.1.1. Laser Ablation Inductively Coupled Plasma Mass Spectroscopy (LA-ICP-MS)

Once the samples had been prepared, 160-micron diameter spots were ablated in selected areas of the tooth and bone using an Agilent 7700 Series LA-ICP-MS. This instrument recorded the number of particles of selected masses Pb-206, Pb-207, Pb-208, Th-232, and U-238 to be used in the isotopic age calculation. The NIST-612 glass and Walnut Canyon carbonate standards were ablated alongside the samples to ensure accuracy (Hollocher et al, 1995; Roberts et al, 2017). The data from the LA-ICP-MS was imported into Iolite software inside of the Igor Pro program. Using this software, baseline measurements of elemental concentrations and mass counts per second were selected and then corrected for machine error using the Geochron-4 Data Reduction Scheme (DRS). The trace elemental composition of both samples was also analyzed using Iolite's Trace Element DRS. Parts-per-million concentrations of Mg, Ca, Sr, Mn, Fe, Th, U, and all of the elements in the lanthanide series were calculated and corrected for in a similar manner. The concentrations of these elements were divided by the calcium concentration

to normalize them, as the primary component of the samples is calcium phosphate. These results were used to assemble a story of the fluid flow history and uranium replacement.

Additional LA-ICP-MS data was recorded to examine smaller sections of the samples with a higher degree of precision. Twenty-five congruent lines situated side by side on a 2-D plane were ablated to form elemental maps of the sections of dentine and enamel for tooth sample 1A, and to map cortical and spongy bone in bone sample 1C. The lines were approximately 8500 μm long, covering the aforementioned sections in a small amount of space. They were ablated 50 μm apart from each other, using a 20 μm diameter laser beam at 10 μm/s speed of laser travel. The laser measured isotopes and calculated isotopic ratios for Pb-206, Pb-207, Pb-208, Th-232, U-238. These ratios were then used to calculate isotopic ages for the different sections of the sample and included in the uptake model.

2.1.2. X-Ray Absorption Near Edge Structure (XANES)

The National Synchrotron Light Source II (NSLS II) was utilized in the tender energy range, 1 to 5 keV, to create a map and determine the speciation of select elements in sample 1A. Chlorine, phosphorus, and uranium were analyzed using an 8 μm beam of electrons, which spanned 10 μm pixels in the resulting images. In the hydroxyapatite mineral which constitutes the tooth and bone sample, Cl is often substituted into the lattice by redox processes, replacing the OH^- component. Therefore, the concentration of Cl gives insight into the reducing conditions of the environment. In addition, uranium was chosen to understand the state of its ions in the samples. Lastly, elemental phosphorus concentrations were chosen as a comparison and normalization point, because it is the component of the hydroxyapatite which is most affected by the electron beam in the tender energy range. Each pixel was struck with the beam for 0.16 seconds each. At 3550 eV, the uranium is most clearly visible and can be used to analyze the near-edge structure of the atoms.

2.2. Synthetic Model Development

To get an accurate age using the age equation, common Pb must be corrected for. Therefore, only the component of the Pb which is a product of decay was compared to the concentrations of U. Because Pb-208 remains at a constant concentration over time, it can be used as an anchor for common Pb correction, a process which removes Pb which has not developed from the decay of U. The ratio of radiogenic Pb-206 to Pb-208 is about 2:1, so a simple equation is created based off this proportion, seen in Equation 3. The radiogenic lead can then be placed into the isotopic age equation for the decay of U-238, provided by Equation 4.

$$Pb^* = {}^{206}Pb - \frac{1}{2}\left({}^{208}Pb\right) \text{ (3)}$$

$$Pb^* = {}^{238}U\left(1 + e^{-\lambda t}\right) \text{ (4)}$$

A model displaying an exponential falloff rate of uptake for uranium was devised based upon the above equation. Where *R(t)* is the rate of uranium uptake at any *t*, time, is equal to the initial uranium uptake rate, A_0, times the constant e with an exponent of time divided by -τ, a variable representing the time in which the rate has decreased by a factor of e. The governing equations are Equations 5 and 6.

$$R(t) = A_0 e^{-t/\tau} \text{ (5)}$$

$$R(\tau) = \frac{A_0}{e} \text{ (6)}$$

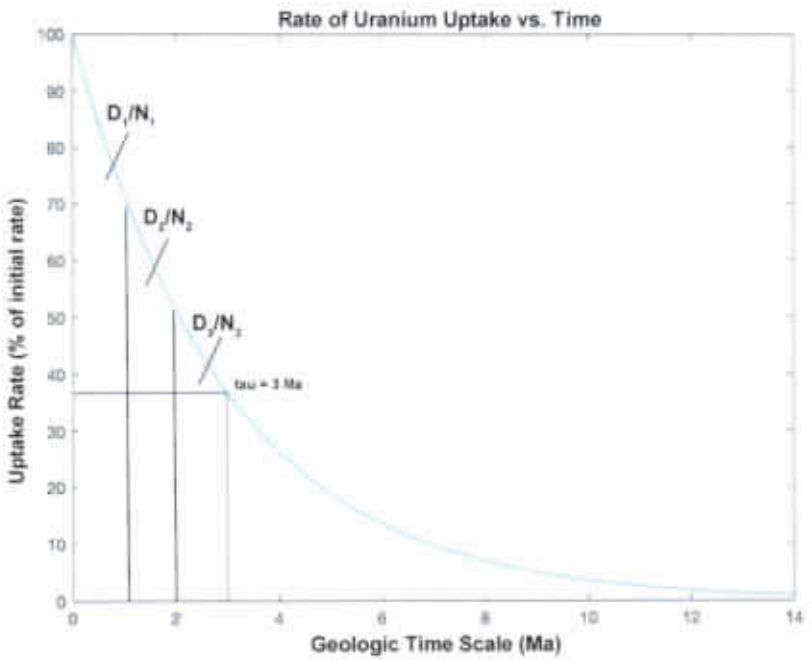

Figure 3. Rate of uranium uptake over a timescale of 14 million years, or the age of the Barstow samples. When the τ is set at 3 Ma, the rate of uptake is given by the initial concentration of uranium over e. D is defined as the number of daughter atoms and N the number of parent atoms.

The model assumes an exponential falloff rate due to the fact that the initial concentration of uranium in the samples was negligible at the time of the animals' deaths, and then would have been rapidly taken up during burial to have led to the state of diagenesis in the samples. Following the initial diagenesis, the rate of uranium uptake must have slowed exponentially due to the decrease in pore space accompanying any precipitation of uranium where there was formerly organic matter.

Taking the integral of the rate equation provides the number of atoms of uranium which are taken up over a given time, as seen in Equations 7 and 8. Related to this, the total number of parent and daughter atoms are described by Equations 9 and 10, respectively.

$$\int_0^t A_0 e^{-t/\tau} \delta t = -\tau A_0 e^{-t/\tau} \quad (7)$$

$$\left[-\tau A_0 e^{-t/\tau}\right]_0^t = -\tau A_0 e^{-\frac{t}{\tau}} + -\tau A_0 = -\tau A_0 \left(1 - e^{-\frac{t}{\tau}}\right) \quad (8)$$

$$N_{total} = \sum_{i=1}^{i=n} \tau A_0 (e^{-t_i/\tau} - e^{-t_{(i+1}/\tau}) * e^{-\lambda(t-t_{i+1})} \quad (9)$$

$$D = \sum_{i=1}^{n} \tau A_0 (e^{-t_i/\tau} - e^{-t_{(i+1}/\tau}) * \left(1 - e^{-\lambda(t-t_{i+1})}\right) \quad (10)$$

The fit of the predicted τ to the data set is given by the addition of the squares of the differences between the predicted and observed values of daughter and parent atoms, as seen in Equation 11.

$$(N_{observed} - N_{predicted})^2 + (D_{observed} - D_{predicted})^2 \quad (11)$$

2.3. Application of Code

This code was designed to read in data collected from individual spots and the full maps measured using the LA-ICP-MS. It calculates the best-fitting τ value for the set of data, indicating the timescale in which the majority of the uranium was taken up in each sample. For given value of τ, the initial input concentration rate, A_0 that satisfies total concentration of both parent and daughter is solved for. The loop predicts the number of parent atoms and number of daughter atoms at the end of 14 Ma for each given sample.

```
tau = linspace(0.5e6,10.0e6,101); lambda = 1.55125e-10; t = 0:0.1e6:14e6; tf = 14e6;
sum = final number of parent (U238) atoms (ppm)
sum2 = final number of daughter (Pb206) atoms (ppm)
total(k) = parent(k)+daughter(k); sum = 0; sum2 = 0;
a0=total(k)/(tau(j)*(1-exp(-tf/tau(j))));
sum = sum + tau(j)*a0*(exp(-t(i)/tau(j))-exp(-t(i+1)/tau(j)))*exp(-lambda*(tf-t(i+1)));
sum2 = sum2 + (tau(j)*a0*(exp(-t(i)/tau(j))-exp(-t(i+1)/tau(j)))*(1-exp(-lambda*(tf-t(i+1)))));
minMatrix = min(total_misfit(:)); [col] = find(total_misfit==minMatrix); tau(col)
```

Figure 4. A sample of the code utilized in the model as described by the equations for D, N, and best fit τ.

3. Results:

3.1. Isotopic Age Data

Concentrations of several isotopes from the uranium series were measured in bone, enamel and dentine, and were then placed into the isotopic age equation for U-238 decay. The tooth and bone individual spot sample set ages are displayed in Figure 5 below. These ages were calculated by a piece of the model code, which read in the values of the number of daughter and parent atoms for each ablated spot and placed them into the isotopic age equation, Equation 4. With a higher proportion of U to Pb, due to uranium uptake, the age becomes younger than the actual age, as less of the parent isotope has decayed into the daughter isotope. On the contrary, when the proportion of U to Pb is lowered due to uranium leaching, the age of the sample becomes older than its true value.

As described previously, the lead concentrations in each sample set were corrected for the presence of common lead, as shown in Equation 3. This ensures that the lead atoms which were present in the samples at the time of burial, and not products of radioactive decay, do not influence the isotopic age.

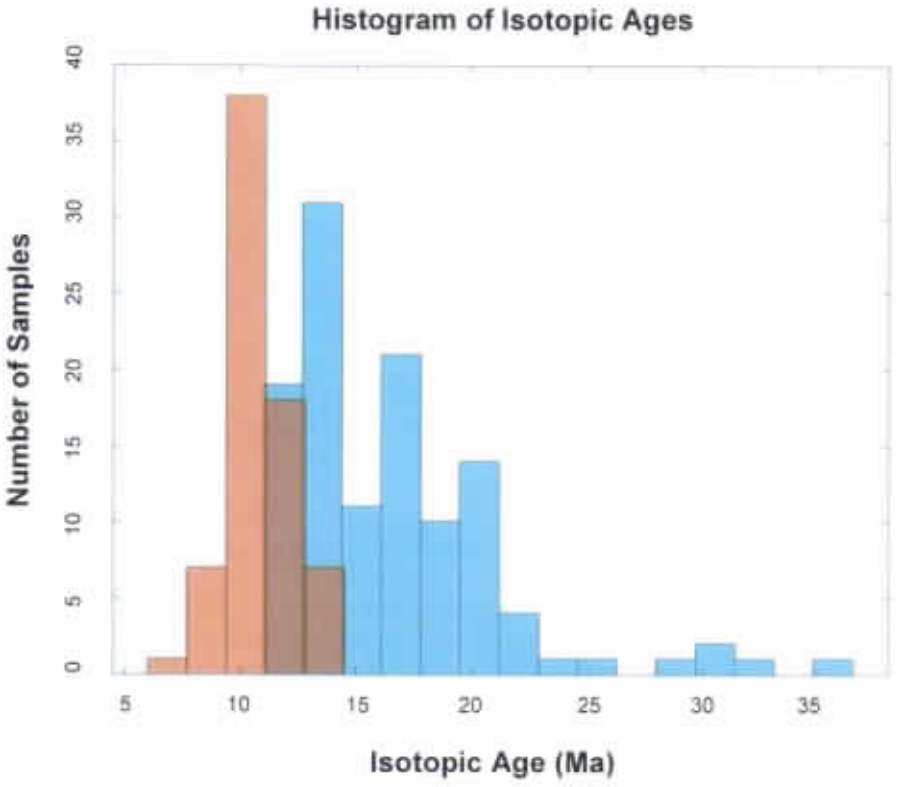

Figure 5. Histogram displaying isotopic ages of the tooth and bone sample sets. The tooth data is represented in blue and the bone data is represented in red.

Table 1. Isotopic ages of the tooth and bone sample sets

Sample	Sample Size	Mean	Median	Standard Deviation
1A: Tooth	117	16.6 Ma	15.7 Ma	4.54 Ma
1C: Bone	71	10.8 Ma	10.7 Ma	1.45 Ma

As seen in Table 1, Sample 1A produced a wider range of data due to the discrepancy in ages between the enamel and dentine sections. Being able to easily take up uranium at the time of burial, the tooth sample displays a median age of 15.7 Ma. When taking account of the difference between the enamel and dentine sections in the tooth, however, the dentine is generally younger and closer to the burial age of 14 Ma. The dentine's porous structure has allowed it to uptake thousands of parts-per-million of uranium since being buried, and therefore displays higher concentrations of the element. In contrast, the enamel sections, taking up little uranium at the time of death, display older ages due to the presumed leaching of uranium from the system. Due to the complex fluid flow history of Southern California, uranium-bearing waters could have had the effect of 1) leaching surface-bound uranium in such a nonporous biomaterial as the enamel of the tooth, and 2) precipitating uranium in the pores of the dentine.

Regarding Sample 1C, the data provides a much more concentrated range of isotopic ages, with a median of 10.7 Ma, and a standard deviation of 1.45 Ma. The tooth's less rigid structure has contributed to its susceptibility to fluid flow events and appears to have continually taken up uranium over time. Due to the presence of excess uranium in comparison to lead, the isotopic age equation assumes that less U-238 has decayed to become Pb-206, therefore determining the sample to be younger than it is biologically.

The ages provided in Table 1 are not consistent with the stratigraphy of the Barstow Formation, and are a byproduct of diagenesis and a continuous uranium uptake history in the sample. Due to the high concentration of uranium in the dentine and spongy bone spot samples, the element is theorized to have been taken up throughout the burial period. This prompted the modeling of an exponential falloff rate of uptake, meaning that at first uranium was rapidly entering the system and slowed exponentially after the burial. To further picture the spatial distribution of uranium and lead in the tooth and bone samples, map images were created utilizing the LA-ICP-MS.

3.2. Laser Ablation Maps

The maps of uranium and lead inside the tooth samples are located below in Figures 6A and 6B. The maps highlight the distinct regions of high and low uranium content inside the sample. In the tooth, the inner dentine and outer dentine display concentrations of uranium in the 1000 - 4000 ppm range. The enamel, however, displays concentration of uranium in the range of 0 - 100 ppm. The lead concentrations are more consistent throughout the sample, therefore when placed into a ratio with the uranium, the dentine displays a higher ratio of uranium to lead, and the enamel a lower ratio of uranium to lead. Additionally, the dentine sections have a greater variation in their isotopic concentrations, highlighting the porosity of the material. The enamel sections are rather uniform in their distribution of isotopes. The dentine layers appear to have taken up uranium in a rapid manner due to the porous material constituting these sections, whereas the enamel may have taken up uranium at a lower rate or have even been leached of the element.

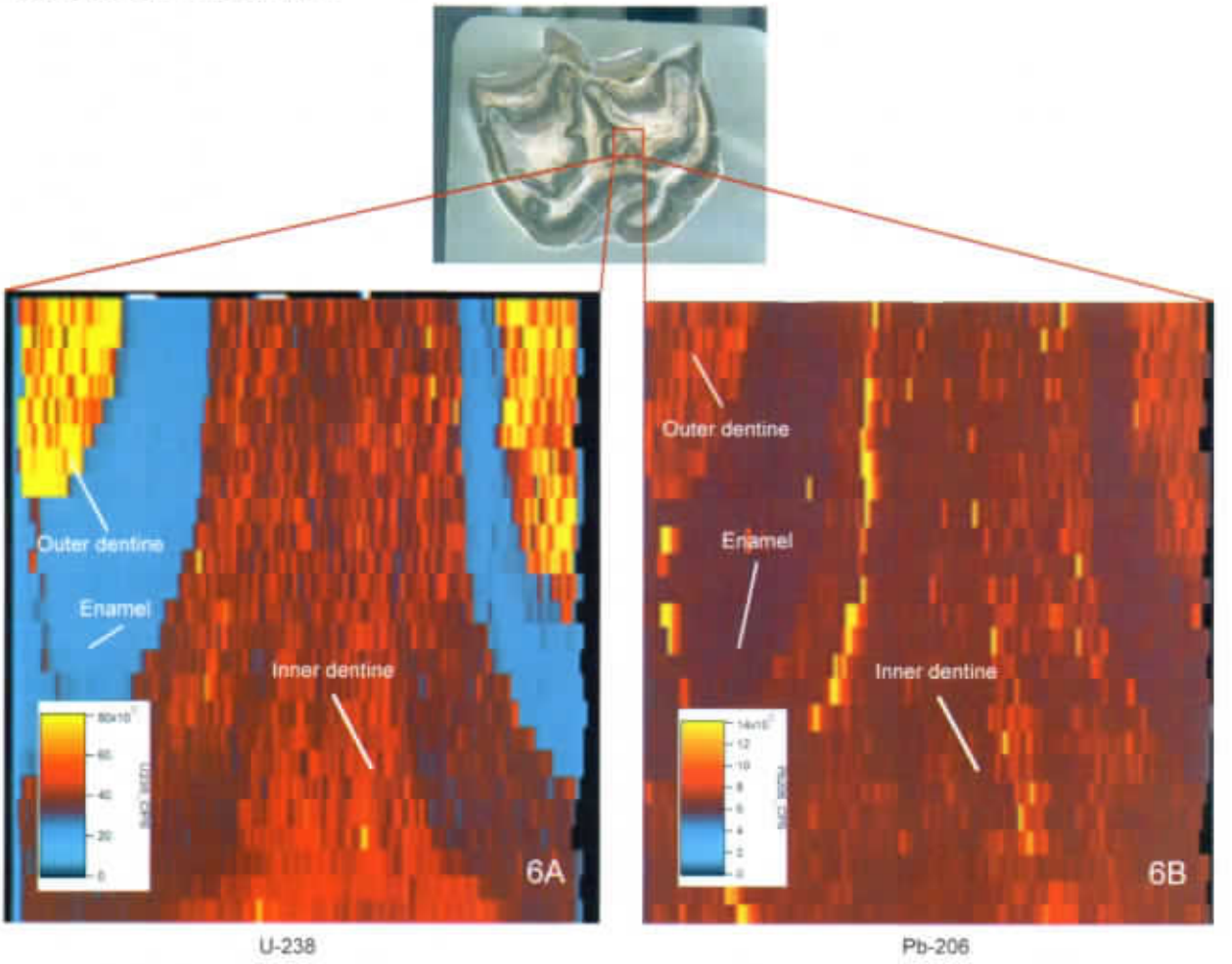

Figures 6A & 6B. 2-Dimensional map images of a tooth sample displaying elemental concentrations of U-238 and Pb-206, respectively. These images are smaller and more precise than the synchrotron because of the small spot diameter size and slow scanning speed of the laser. The concentration of uranium is highly distinct to each section (inner dentine, inner enamel, outer dentine). The lead is fairly homogeneous.

The maps of bone sample 1C display a similar divided pattern of uranium when comparing sections of spongy bone and of the pore spaces, as seen in Figures 7A and 7B. The spongy bone appears to have taken up a large amount of uranium in a similar manner as the dentine, having a U concentration range of 2000–4000 ppm. This indicates that the rate of uptake was rapid at the time of burial, and exponentially ceased thereafter. The pore spaces where organic matter was formerly present appear to have been mineralized rapidly following the burial of the horse. Most likely, the spaces containing both organic matter and calcium phosphate surrounding the pores took up the most uranium when the organic matter initially decayed by producing a reducing environment key to the uranium's incorporation into the structure of the biomaterial.

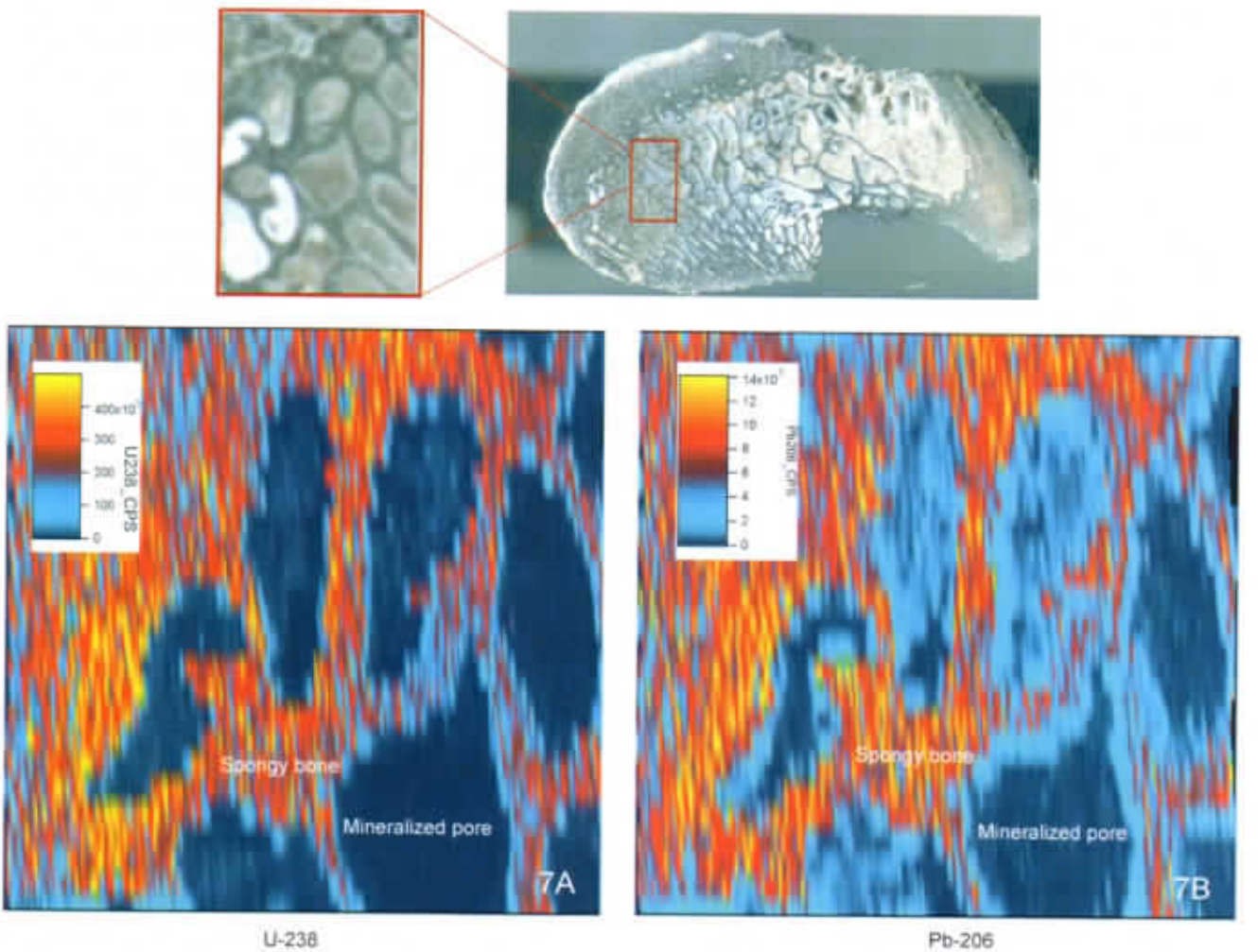

U-238 Pb-206

Figures 7A & 7B. 2-Dimensional map images of a bone sample displaying elemental concentrations of U-238 and Pb-206 respectively. These images are smaller and more precise than the synchrotron because of the small spot diameter size and slow scanning speed of the laser. The concentration of uranium is highly distinct to each section (spongy bone, mineralized pore).

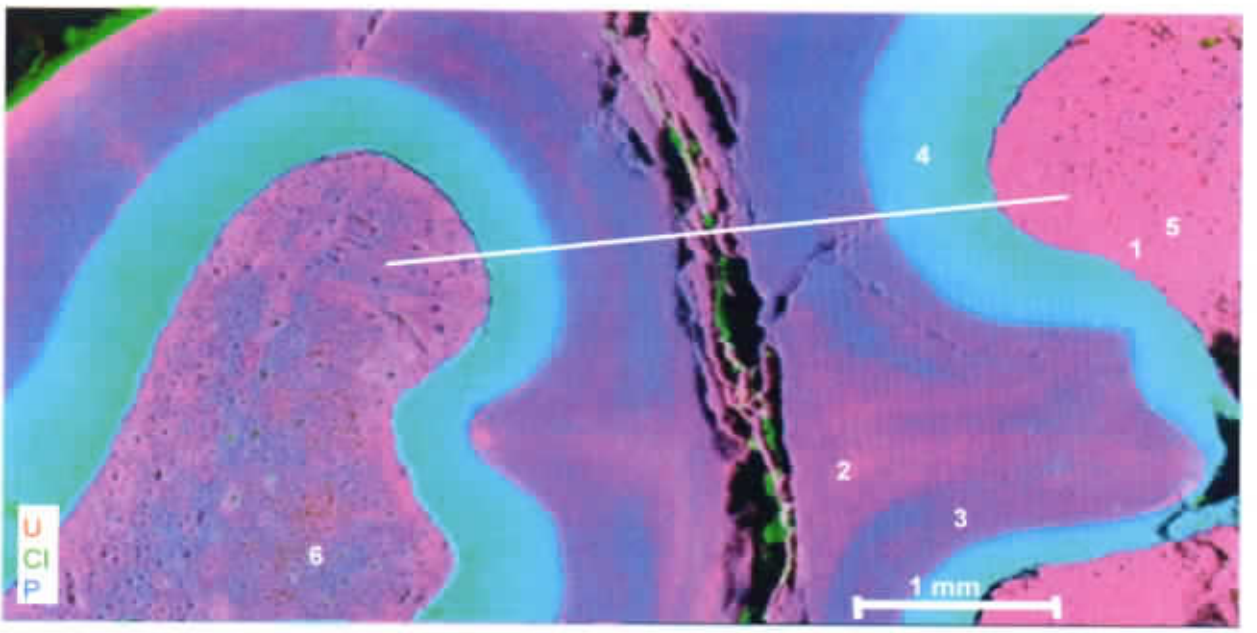

Figure 8. A partial image of sample 1A which depicts the relative concentrations of uranium, chlorine, and phosphorus atoms. U is pictured in red, Cl in green, and P in blue, respectively. Several localities were chosen for XANES analysis, and the numbers are indicated in the figure. A line is shown to indicate the location in which relative concentrations are graphed in Figure 9.

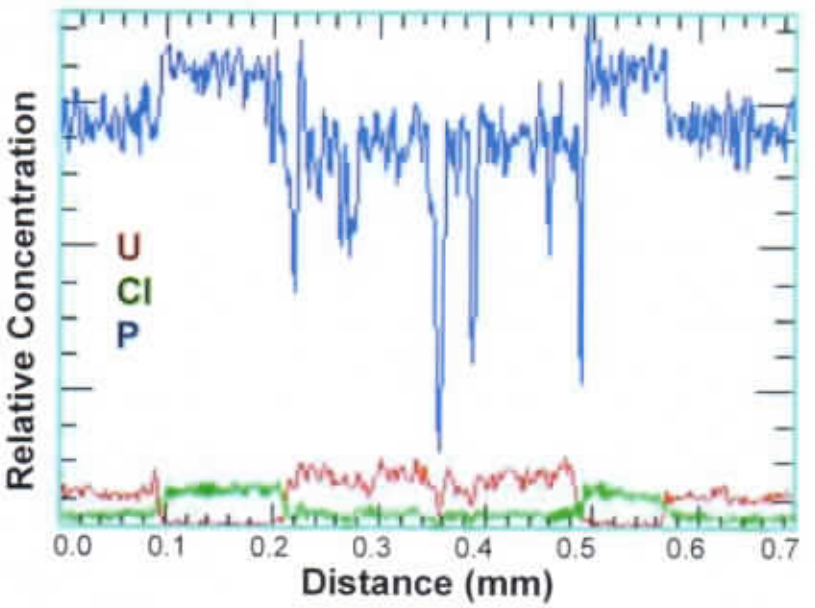

Figure 9. The relative concentration over the distance of the sampled line of U, Cl, and P.

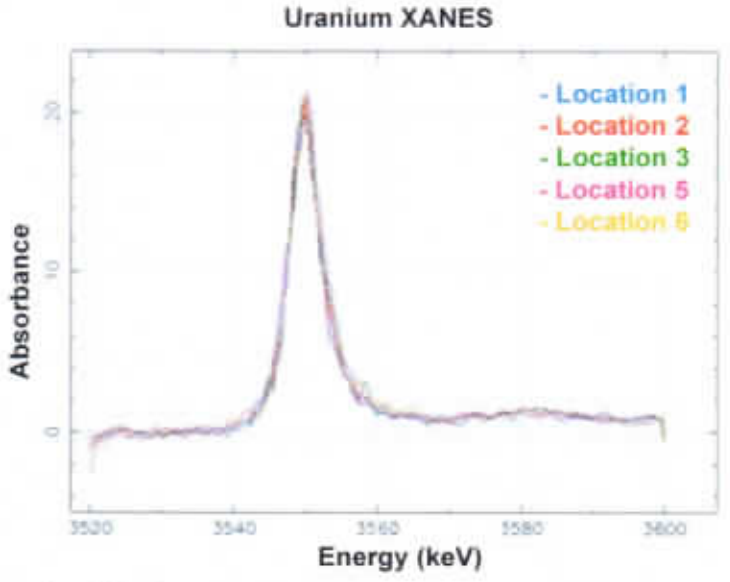

Figure 10. The XANES results which show absorbance of uranium atoms at all locations at 3550 eV.

Tender Energy Spectroscopy determined that uranium is in the U(VI) form in this tooth sample, which indicates that uranium is oxidized. The tooth contains primarily the mineral hydroxyapatite, a form of calcium phosphate, which is why the concentration of phosphorus is so great in the sample. In the mineral lattice, Cl is a substitute for a component of the phosphate, indicating where the concentration of phosphate is the highest. The huge enrichment of uranium in the sample could be associated with organic matter, as reducing conditions can be created when organic matter decays.

Along the line shown in Figure 8, sections of inner dentine, enamel, outer dentine, enamel, and inner dentine are passed through in order from left to right. This figure indicates that the concentration of uranium is greatest where the phosphate is at a relative low concentration. Specifically, in the inner dentine, concentrations of Cl and P are lowered, and U is elevated. This suggests that uranium has effectively filled a large portion of the pores, replacing calcium ions. In the enamel, concentrations of U are low, and therefore by comparison Cl and P are high. Lastly, the outer dentine displays similar patterns to the inner dentine.

In the localities provided in Figure 8, the state of uranium is the exact same, oxidized and in the U(VI) form. At 3550 keV, the U(VI) ion absorbs the electrons from the synchrotron and becomes excited, as shown in Figure 10 (Duff et al, 1997). There is no shift away from this energy level at any of the localities, demonstrating the consistency of uranium's state throughout the sample. Therefore, the enamel, outer dentine, and inner dentine contain oxidized uranium solely.

4. Discussion:

4.1. Model Confirmation with Synthetic Data

Utilizing the maps of the teeth and bone samples, an exponential falloff model was devised to simulate the rate of uptake of uranium. The τ value describes the time in which the rate of U uptake has decreased by a factor of e. A constructed value of τ, designated at 3 Ma, and U uptake rate were placed into the model to determine its efficacy. The model produced a residual for predicted daughter and parent concentrations, which was compared to the synthetic τ value. As seen in Figure 11, the synthetic τ produced with the least total misfit was graphed at 3 Ma, confirming the ability of the model to predict the best fit τ.

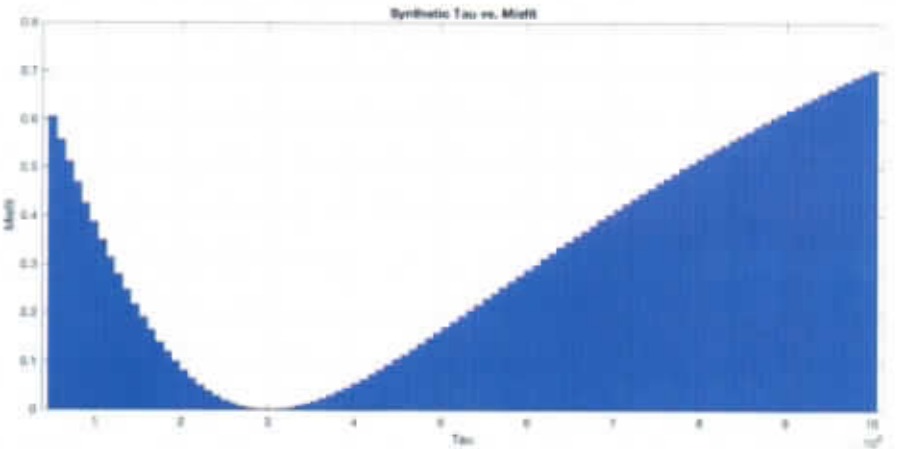

Figure 11. Synthetic output of τ yielded the least total misfit at approximately 3 Ma, which matched the input τ.

To confirm the model's ability to predict τ from isotopic ratios, the τ value produced from the model was used to predict the apparent age of the constructed data. The age output for this value of τ is 11 Ma, consistent with the true age of the synthetic data, based upon the ratio of U to Pb, seen in Figure 12.

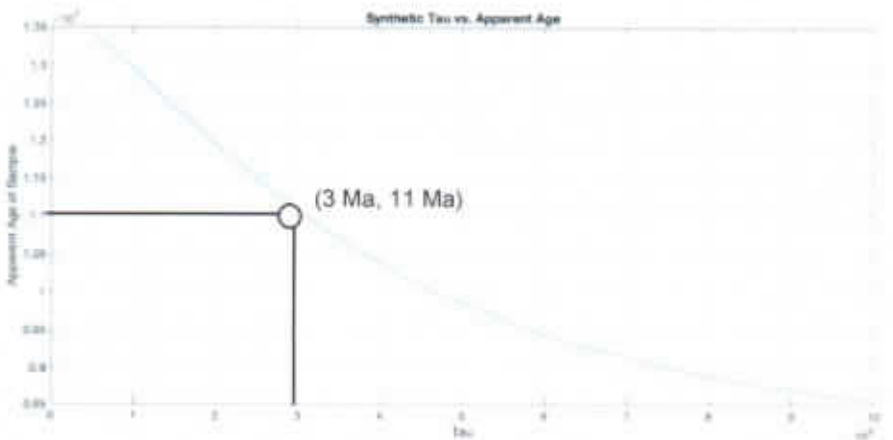

Figure 12. Synthetic output of τ yielded the least total misfit at approximately 3 Ma, which gives an apparent age for the sample of about 11 Ma.

4.2. Tau Prediction for Bone Sample

The aforementioned τ value indicates the manner of uranium uptake in a sample, with a large τ symbolizing a prolonged period of uptake and a small τ specifying rapid initial uptake with a quick falloff. The model utilized isotopic information from seventy-one spots in the spongy bone region of sample 1C to produce a best fitting τ value for the data. Based upon this data, the least residual value between the sum of the squares of observed and predicted parent and daughter concentrations, written in Equation 11, occurs when the τ value is 1.3 Ma after the burial of the bone sample, shown in Figure 13.

This indicates that the bone sample underwent rapid diagenesis resulting in its preservation and the inclusion of thousands of parts-per-million of uranium atoms into its hydroxyapatite structure. 1.3 Ma after the burial of the animal, the rate of uptake had decreased by a factor of 1/e. Subsequently, the model predicts the correct age of burial of the sample, around 14 Ma, as shown in Figure 14. In addition, Figure 14 provides insight into the systematics of τ with regard to burial age, with a tradeoff taking place between these variables. If the τ value were greater than 2 Ma, an incorrect age would be predicted for the time of burial, ranging from 15 to 20 Ma. This confirms that the model is effective for predicting the systematics of uranium uptake in a preserved fossil bone and demonstrates this biomaterial's ability to sequester uranium over a timescale of 14 Ma. If a material similar to this porous phosphate were used to remediate nuclear waste, it would remain effective over a timescale of millions of years.

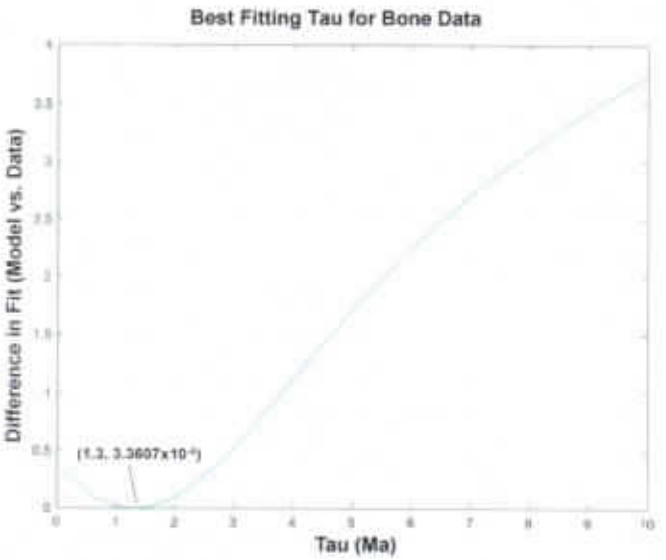

Figure 13. Utilizing information from seventy-one spots of spongy bone material, the model predicted that the τ value fits the data best when placed at 1.3 Ma into the burial of the bone.

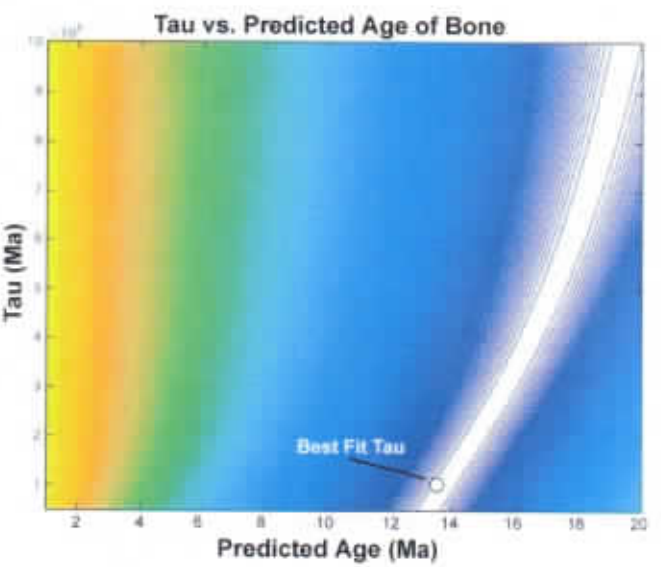

Figure 14. Searching through values of τ for a predicted age reveals a tradeoff between the τ value and the predicted age, however with the best fitting τ set at 1.3 Ma, the predicted date of burial for the bone sample is 14 Ma.

4.3. Tau Prediction for Tooth Sample

With 117 spots spanning the materials of outer dentine, inner dentine, and enamel with sample 1A, the model produced a best-fitting τ at 0.9 Ma after the burial of the horse, shown in Figure 15. Similarly to the bone, rapid diagenesis altered the chemical structure of the hydroxyapatite within the tooth, incorporating oxidized uranium into the lattice in the dentine materials. After 0.9 Ma of uptake, the rate of uranium incorporation slowed by a factor of 1/e. Furthermore, the model again predicts the correct age of burial of the sample, 14 Ma, pictured in Figure 16. This confirms that the model is effective for predicting the systematics of uranium uptake in a preserved fossil tooth and demonstrates the dentine's ability to sequester uranium over a timescale of 14 Ma. The enamel demonstrates how porosity factors into the ability of a remediation material to be effective, as it did not have the capability to take up more than one hundred parts-per-million of uranium in its geologic history.

In comparison with the bone sample, the tooth sample took up its uranium at a slightly more rapid rate, with the e-folding time being 0.9 Ma, and the bone's e-folding time being 1.3 Ma. The dentine and spongy bone biomaterials have the ability to absorb large quantities of uranium in a short period of time and would effectively sequester uranium waste for millions of years.

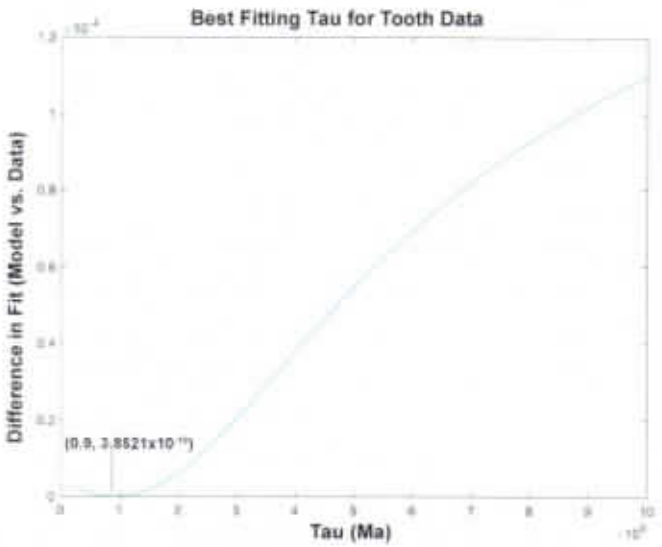

Figure 15. Utilizing information from 117 spots of enamel and dentine materials, the model predicted that the τ value fits the data best when placed at 0.9 Ma into the burial of the tooth.

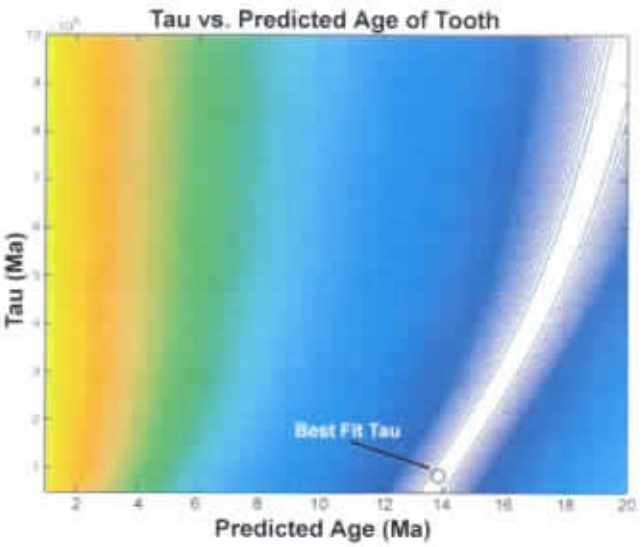

Figure 16. Searching through values of τ for a predicted age reveals a tradeoff between the τ value and the predicted age, however with the best fitting τ set at 0.9 Ma, the predicted date of burial for the tooth sample is around 14 Ma.

5. Conclusion:

5.1. Long-Term Uranium Waste Storage in Phosphates

By taking advantage of preserved geologic samples, a history of uranium uptake was determined for a 14-million-year-old *Scaphohippus intermontanus* horse tooth and foot bone. The uptake of uranium was simulated in the hydroxyapatite fossils, predicting the timeline of radioactive waste immobilization.

With both materials being buried at approximately 14 Ma and immediately undergoing diagenesis, the rate of uranium uptake in the bone decreased by a factor of 1/e in 1.3 Ma, and the tooth by the same factor in 0.9 Ma. Both uptake histories describe the ability of porous phosphates, such as the hydroxyapatite structure which constitutes mammalian teeth and bones, to retain high concentrations of uranium for long periods of time. In the case of the spongy bone, 3000-4000 ppm of U was stored in the biomaterial surrounding mineralized pores for the entirety of the timescale following its burial, with little evidence of leaching. Similarly, the dentine material present in the tooth sample was able to sequester 1000-2000 ppm of U for a similar time period. By contrast, the enamel material of the tooth only held 0-100 ppm of U and shows evidence of U leaching due to its older isotopic age. Based upon this, an integral aspect of uranium immobilization in phosphates is the porosity of the sequestering material, as a phosphate with a large volume of pore space can immobilize the largest quantities of uranium waste.

Impressively, the experimental samples have undergone the highly active tectonic history of Southern California over the last 14 Ma and serve as great examples of the phosphate retention of uranium matter during fluid flow events. The uranium which has become immobilized in the hydroxyapatite samples has not dissolved in the permeating waters and the state of preservation of the micropores is remarkable. A material which is similar to the porous hydroxyapatite could be used as an effective remediator, instead of employing the expensive borosilicate glass and titanium alloy being tested by the Yucca Mountain Site Characterization Project.

The process by which uranium entered the systems is the U(VI) reaction with the hydroxyapatite mineral to become incorporated into the lattice structure. An oxidized state is present in the tooth sample as demonstrated by the XANES results, as U(IV) would be present in a sample with reducing conditions. The sequestration of U may first complex with ligands in the lattice and then become reduced. Due to the enormous affinity phosphate, a porous material such as dentine or spongy bone, has for uranium, it may be most effective in remediating nuclear waste.

5.2. Future Research

Proposed improvements to the model would include the separation of enamel and dentine data for more specific prediction of τ and the inclusion of additional uptake scenarios. While the exponential

falloff rate has proven to match the case study sample set's values of daughter and parent atom concentrations, the possibility of several defining uptake events should be taken into account. Furthermore, more experimentation in the field of uranium speciation would provide better insight into the processes by which oxidized uranium precipitates or incorporates into the mineral lattice.

References:

Banning, A., Demmel, T., Rüde, T. R., & Wrobel, M. (2013). Groundwater uranium origin and fate control in a river valley aquifer. *Environmental Science & Technology*, *47*(24), 13941-13948.

Crowley, K. D. (1997). Nuclear waste disposal: the technical challenges. *Physics Today*, *50*(6), 32-39.

Duff, M. C., Amrhein, C., Bertsch, P. M., & Hunter, D. B. (1997). The chemistry of uranium in evaporation pond sediment in the San Joaquin Valley, California, USA, using X-ray fluorescence and XANES techniques. *Geochimica et Cosmochimica Acta*, *61*(1), 73-81.

Gdowski, G. E. (1997). *Degradation mode survey candidate titanium-base alloys for Yucca Mountain project waste package materials. Revision 1* (No. UCRL-ID-121191-Rev. 1). Lawrence Livermore National Lab., CA (United States).

Gin, S., Abdelouas, A., Criscenti, L. J., Ebert, W. L., Ferrand, K., Geisler, T., ... & Marra, J. C. (2013). An international initiative on long-term behavior of high-level nuclear waste glass. *Materials Today*, *16*(6), 243-248.

Hellstrom, J., Paton, C., Woodhead, J., & Hergt, J. (2008). Iolite: software for spatially resolved LA-(quad and MC) ICPMS analysis. *Mineralogical Association of Canada short course series*, *40*, 343-348.

Hirata, T., & Nesbitt, R. W. (1995). U-Pb isotope geochronology of zircon: Evaluation of the laser probe-inductively coupled plasma mass spectrometry technique. *Geochimica et cosmochimica Acta*, *59*(12), 2491-2500.

Hollocher, K., & Ruiz, J. (1995). Major and trace element determinations on NIST glass standard reference materials 611, 612, 614 and 1834 by inductively coupled plasma-mass spectrometry. *Geostandards Newsletter*, *19*(1), 27-34.

Martinez, R. J., Beazley, M. J., & Sobecky, P. A. (2014). Phosphate-mediated remediation of metals and radionuclides. *Advances in Ecology*, *2014*.

Mathews, T., Beaugelin-Seiller, K., Garnier-Laplace, J., Gilbin, R., Adam, C., & Della-Vedova, C. (2009). A probabilistic assessment of the chemical and radiological risks of chronic exposure to uranium in freshwater ecosystems. *Environmental Science & Technology*, *43*(17), 6684-6690.

Paton, C., Hellstrom, J., Paul, B., Woodhead, J., & Hergt, J. (2011). Iolite: Freeware for the visualisation and processing of mass spectrometric data. *Journal of Analytical Atomic Spectrometry*, *26*(12), 2508-2518.

Pike, A. W., & Hedges, R. E. (2001). Sample geometry and U uptake in archaeological teeth: implications for U-series and ESR dating. *Quaternary Science Reviews*, *20*(5-9), 1021-1025.

Roberts, N. M., Rasbury, E. T., Parrish, R. R., Smith, C. J., Horstwood, M. S., & Condon, D. J. (2017). A calcite reference material for LA-ICP-MS U-Pb geochronology. *Geochemistry, Geophysics, Geosystems*, *18*(7), 2807-2814.

Sanding, A., & Bruno, J. (1992). The solubility of (UO2) 3 (PO4) 2· 4H2O (s) and the formation of U (VI) phosphate complexes: their influence in uranium speciation in natural waters. *Geochimica et Cosmochimica Acta*, *56*(12), 4135-4145.

Sharp, J. O., Lezama-Pacheco, J. S., Schofield, E. J., Junier, P., Ulrich, K. U., Chinni, S., ... & Giammar, D. E. (2011). Uranium speciation and stability after reductive immobilization in aquifer sediments. *Geochimica et Cosmochimica Acta*, *75*(21), 6497-6510.

Wang, Y., Cerling, T. E., & MacFadden, B. J. (1994). Fossil horses and carbon isotopes: new evidence for Cenozoic dietary, habitat, and ecosystem changes in North America. *Palaeogeography, Palaeoclimatology, Palaeoecology*, *107*(3-4), 269-279.

Wellman, D. M., Glovack, J. N., Parker, K., Richards, E. L., & Pierce, E. M. (2008). Sequestration and retention of uranium (VI) in the presence of hydroxylapatite under dynamic geochemical conditions. *Environmental Chemistry*, *5*(1), 40-50.

Woodburne, M. O., Tedford, R. H., & SWISHER III, C. C. (1990). Lithostratigraphy, biostratigraphy, and geochronology of the Barstow Formation, Mojave Desert, southern California. *Geological Society of America Bulletin*, *102*(4), 459-477.